Spatiotemporal Seismic Risk Assessment of Wood-frame Houses in Victoria, Canada under M9 Megathrust Subduction Sequences

Lizhong Zhang
PhD Candidate, Dept. of Civil Engineering, University of Bristol, Bristol, United Kingdom

Katsuichiro Goda
Associate Professor, Dept. of Earth Sciences, Western University, London, Canada

ABSTRACT: This study assesses spatiotemporal seismic risk of a realistic portfolio of wood-frame houses in the City of Victoria, British Colombia, Canada, subjected to a M9 sequence of earthquakes originating from the Cascadia subduction zone in Pacific Northwest. Crustal aftershocks, triggered by the mega-thrust mainshock, may occur in much proximity to population and buildings, and different types of buildings may be affected due to different ground-motion characteristics. The developed time-dependent seismic risk model consists of an Epidemic Type Aftershock Sequence model, ground-motion model, and aftershock seismic fragility model. The seismic hazard model for synthetic mainshock-aftershock sequences is combined with the state-dependent fragility model to estimate time-dependent damage states of wood-frame houses. The output of the assessment is useful for making various risk management decisions more effectively.

1. INTRODUCTION

Recent earthquake sequences, such as the 2010-2011 Darfield-Christchurch and the 2011 Tohoku sequences, showed the destructive effects of aftershocks on buildings. The cumulative damage due to aftershocks can have an impact on the post-earthquake risk assessment immediately after the mainshock (Nazari *et al*. 2013; Ebrahimian *et al*. 2014; Iervolino *et al*. 2014).

According to the turbidite records in the past 10,000 years, the Cascadia subduction zone (CSZ) has ruptured 19 times (Goldfinger *et al.* 2012). The current best estimate of the return period for M9 events in the CSZ is 526 years and the last event occurred in 1700. On the other hand, Ventura *et al*. (2005) indicated that 56% of buildings in British Columbia are wood-frame houses, 40% of which were built before 1970. Since seismic provisions of the National Building Code of Canada were adopted and enforced in British Columbia after 1973, the seismic resistance of old residential houses is low. Consequently, many wood-frame houses may suffer significant damage due to a M9 mainshock-aftershock sequence in the CSZ.

An Epidemic Type Aftershock Sequence (ETAS) model is widely used in statistical seismology to model the seismicity rate in space and time. Applications of the ETAS model for shallow crustal seismicity have been investigated extensively (Seif *et al*. 2017). Parameters of the ETAS model can be estimated from selected instrumental catalogs, and the calibrated model can simulate synthetic catalogs. Zhang *et al*. (2018) developed the ETAS simulation approach for the M9-class mega-thrust subduction earthquake sequence and applied it to a case study in Japan. The new simulation approach showed a good agreement with the seismicity and hazard rates of the 2011 Tohoku sequence. However, since the aftershock fragility curves are not available in Japan, they did not discuss the effect of mainshock-aftershock sequences on cumulative damage in the risk assessment.

In earthquake engineering, Luco *et al*. (2004) developed aftershock fragility curves for a steel moment-resisting frame for California using 30 mainshock records. They generated the aftershock

records from the scaled mainshock records and performed incremental dynamic analysis (IDA). On the other hand, Li and Ellingwood (2007) found that the scaled mainshock records as aftershock records overestimated drift ratios of steel moment frame buildings, whereas Raghunandan *et al*. (2015) pointed out the computational challenge of Luco *et al*.'s back-to-back approach. Goda and Salami (2014) investigated the impact of aftershocks of wood-frame houses using a seismic analysis of wood-frame structure (SAWS) model (Folz and Filiatrault 2004; White and Ventura 2006) for Canada. Their results showed aftershocks contributed additional 5%-20% damage in comparison with the mainshock. However, the effects of cumulative damage due to aftershocks were not taken into account.

This study conducts a spatiotemporal seismic hazard and risk assessment for a M9 earthquake sequence in the CSZ. The ETAS simulation framework from Zhang *et al.* (2018) is applied to the City of Victoria, British Colombia, Canada given a M9 subduction earthquake occurs in the CSZ. To assess the cumulative damage of the wood-frame houses due to the mainshock-aftershock sequences, a new method to develop aftershock fragility curves is applied to the SAWS model using extensive mainshock-aftershock ground-motion records (Goda and Taylor 2012; Goda *et al.* 2015). A real building dataset in the City of Victoria is applied to estimate the damage states in different time intervals after the mainshock. The novelties of this study are that (1) a new method is developed to produce the aftershock fragility curves, which avoid the overestimation of EDP (engineering demand parameter) and the high computation cost from the back-to-back approach, and (2) the effect of triggered aftershocks by M9 events on spatiotemporal seismic hazard and risk assessment is investigated. The output of this study can be further applied to scenario-based post-earthquake risk assessment, inspection prioritization, and building tagging.

In the following, the framework for the spatiotemporal seismic hazard and risk assessment is described in Section 2. The application of the ETAS model for the CSZ is given in Section 3. The results of the seismicity rate are illustrated in Section 3.1. Ground motion perdition equations (GMPEs) are used to calculate the daily hazard rate in Section 3.2. After developing the aftershock fragility curves in Section 3.3, the risk assessment for the City of Victoria is carried out in Section 3.4.

2. ASSESSMENT FRAMEWORK

The overall framework of the spatiotemporal seismic hazard and risk assessment is shown in Figure 1. It consists of the seismicity model, seismic hazard model, and fragility model. Synthetic catalogs from the ETAS simulation provide the time, magnitude, and location of mainshock-aftershock sequences. Subsequently, GMPEs are applied to the synthetic catalogs to estimate the daily hazard rate at different sites. Next, the daily hazard rates can be used to evaluate the damage states at different time-intervals after the mainshock.

2.1. ETAS model

The total rate $\lambda(t,x,y|H_t)$ of the ETAS model (Seif *et al*. 2017) includes a background rate $\mu(x,y)$ and a triggering rate $g(t-t_j, x-x_j, y-y_j; M_j)$:

$$\lambda(t,x,y|H_t) = \mu(x,y) + \sum_{j:t_j<t} g(t-t_j, x-x_j, y-y_j; M_j) \quad (1)$$

where H_t are the historical seismicity up to time t ($H_t = \{x_j, y_j, t_j, M_j\}$; $t_j<t$). The triggering function $g(t,x,y;M)$ consists of the productivity ($K_0\, e^{\alpha(M-M_{cut})}$), the normalized modified Omori function $c^{p-1}(t+c)^{-p}(p-1)$, and a spatial distribution of seismic events:

$$g(t,x,y;M) = K_0\, e^{\alpha(M-M_{cut})} \cdot c^{p-1}(t+c)^{-p}(p-1) \cdot \frac{(q-1)}{\pi(x^2+y^2+d\, e^{\gamma(M-M_{cut})})}\left(1+\frac{x^2+y^2}{d\, e^{\gamma(M-M_{cut})}}\right)^{-q} \quad (2)$$

where M_{cut} is the cut-off magnitude. K_0 and α are the productivity parameters; c and p are the

temporal parameters; and d, q, and γ are the spatial parameters.

Since the observed M9 sequence is not available for the CSZ, and the last M9 event occurred in 1700 (Goldfinger *et al.* 2012), the productivity parameters (K_0 and α) are taken from Zhang *et al*. (2018) based on the seismicity analysis in Japan. The temporal and spatial parameters are estimated from the NEIC catalog in the CSZ. The ETAS parameters are K_0 = 0.064±0.021, α = 2.3, c = 0.006±0.005, p = 1.204±0.098, γ = 1.112±0.452, d = 17.33±17.07 and q = 1.934±0.348.

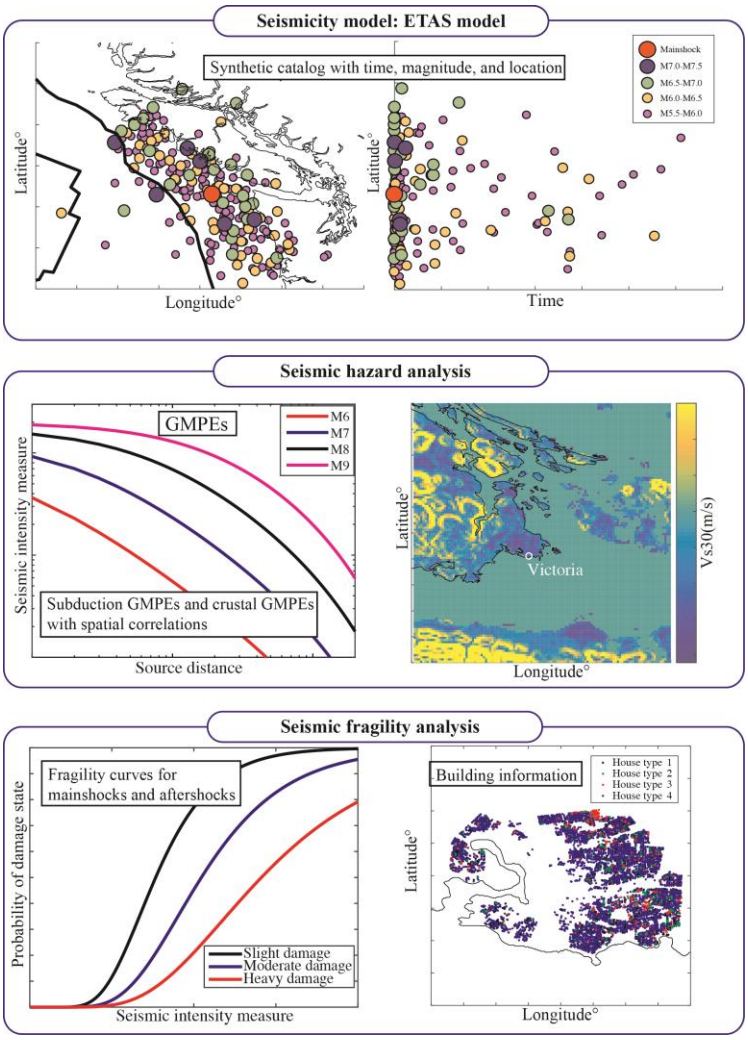

Figure 1.Overall framework of the spatiotemporal seismic hazard and risk assessment.

The geometry of the rupture area is constrained by different down-dip edge models as suggested by the Geology Survey of Canada and the 2014 United States National Seismic Hazard Map (Petersen *et al*. 2014) for the CSZ.

2.2. Seismic hazard analysis

To compute scenario-based shake maps of M9 earthquake sequences for the City of Victoria, the following GMPEs and V_{s30} information are used. The GMPEs by Abrahamson *et al.* (2016) and Boore *et al.* (2014) are selected to compute the intensity measure (IM) for subduction and crustal earthquakes, respectively. The spatial correlations of subduction and crustal earthquakes are applied as suggested by Goda and Atkinson (2010). In comparison with other GMPEs from the NGA-West2, the GMPE by Boore *et al.* (2014) requires

less input information (e.g., fault type and hanging wall effect), which is more suitable for southwestern British Colombia. The V_{s30} map of the City of Victoria is taken from Allen and Wald (2009).

2.3. Seismic fragility analysis

The aftershock fragility curves are developed using the SAWS model with an extended ground motion database. Sa(T=0.3s) is considered as IM in the risk analysis, because the fundamental period of the SAWS model is 0.3s. More details of the development of the aftershock fragility curves are given in Section 3.3.

The wood-frame houses are classified by the construction year. Four different house types are considered based on Goda *et al.* (2011): (1) House 1 - after 1991, (2) House 2 - from 1981 to 1990, (3) House 3 - from 1971-1980, and (4) House 4 - before 1970. The house classification relates to the seismic resistance of the houses in British Colombia.

3. APPLICATION: VICTORIA CASE STUDY

3.1. ETAS model

The ETAS simulation framework by Zhang *et al.* (2018) is applied to the CSZ . In total, 10,000 one-year synthetic catalogs are generated. The magnitude frequency distribution and the daily number of events are shown in Figure 2. The aftershock seismicity rate with M≥5.5 is high immediately after the mainshock and gradually decays after day 5.

3.2. Seismic hazard analysis

The earthquake events in the synthetic catalogs are applied to the GMPEs with the spatial correlation model (Goda and Atkinson 2010) to generate seismic intensity maps of the City of Victoria. According to the building classification in Section 2.3, the numbers of Houses 1-4 are 387, 197, 257, and 5869, respectively. The grid size of 500m×500m is considered. Subsequently, the IM of each house location is interpolated. An example of daily exceeding hazard rate with Sa(T=0.3s) > 0.5g at the grid site (48.410ºN, 123.346ºW) with V_{s30} = 338m/s is shown in Figure 3.

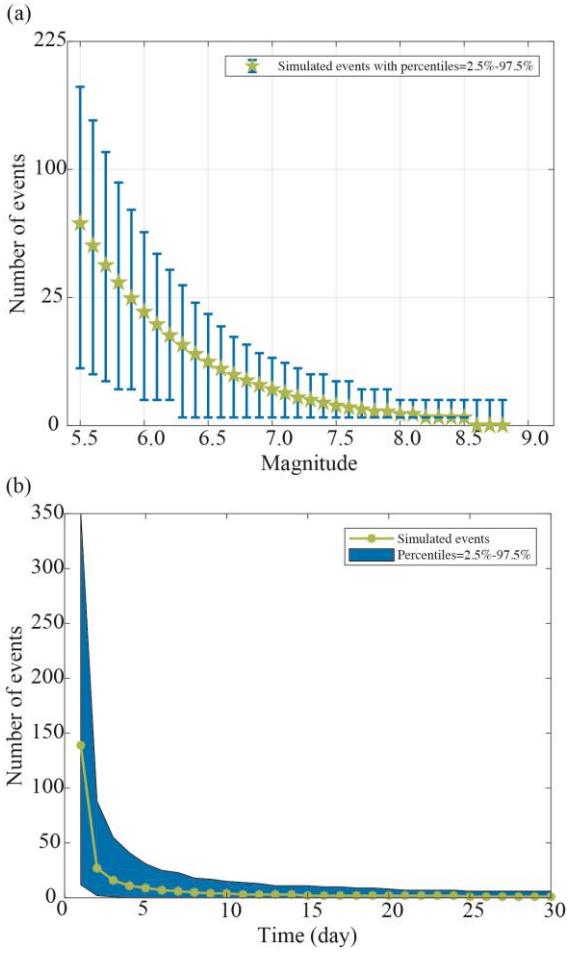

Figure 2. (a) Simulated magnitude frequency distributions of aftershocks. (b) Daily number of simulated events over a month after the mainshock.

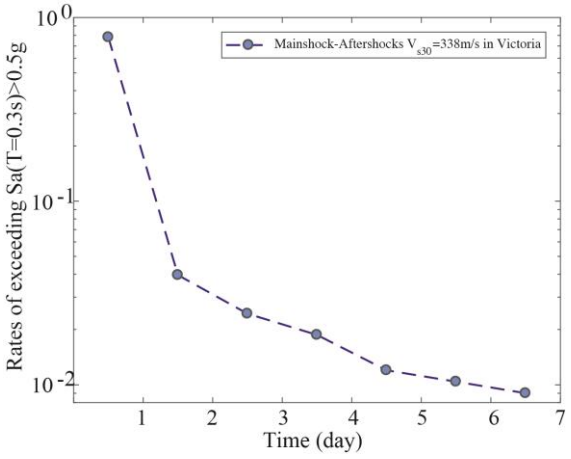

Figure 3. Daily hazard rates of Sa(T=0.3s)>0.5g in Victoria (48.410ºN, 123.346ºW) with V_{s30}=338m/s.

3.3. Aftershock fragility curves

The aftershock fragility curves are developed to assess the cumulative damage due to the mainshock-aftershock sequence. Although the same SAWS models are implemented as in Goda and Salami (2014), the fragility model improves the previous work in several aspects. Firstly, a large number of ground records from real mainshock-aftershock sequences are considered in this study (596 versus 290 ground-motion sequences). Especially, the updated records include the 2011 Tohoku sequences. Secondly, to reduce the computation cost of IDA, the cloud analysis is applied in this study with the extended ground motion records. Scaling factors 1-5 are applied as suggested by Goda and Salami (2014).

To show that the ground motion record selection is appropriate, the comparison of the plot of Sa(T=0.3s) and the maximum inter-story drift ratio (MaxISDR) between this study and Goda and Salami (2014) is shown in Figure 4. The IM-EDP plots of the two studies show a good agreement. However, the IDA results from Goda and Salami (2014) predict slightly higher damage with MaxISDR<2%. This is because the current study includes more mainshock-aftershock records in comparison with Goda and Salami (2014).

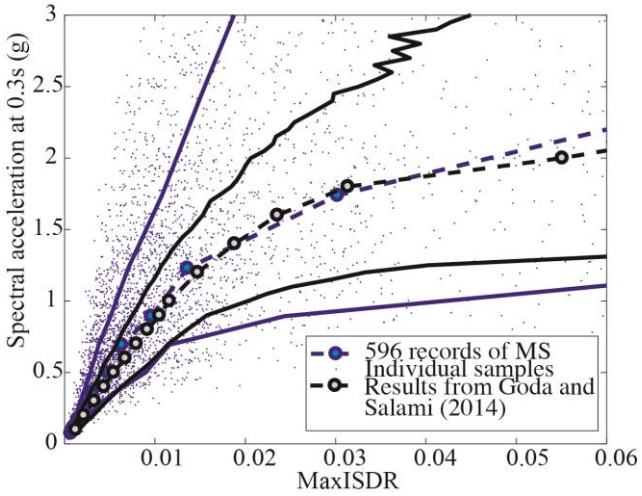

Figure 4. Comparison of the plot of MaxISDR and Sa(T=0.3s) between this study and Goda and Salami (2014).

A new seismic fragility that can account for damage accumulation due to successive ground motions is developed. The fragility model characterizes an inter-dependent relationship among pre-EDP, IM, and post-EDP. The residual inter-story drift ratio (ResISDR), Sa(T=0.3s), and MaxISDR are considered as pre-EDP, IM, and post-EDP for the fragility curve fitting.

FEMA (2000) defined ResISDRs with 0.25%, 1%, and 3% as Immediate Occupancy, Life Safety, and Collapse Prevention, respectively for wood shear walls. For a four-story reinforced concrete building, Uma *et al.* (2010) suggested that 0.2% ResISDR may be taken as serviceability limit, whereas 0.4%-0.6% ResISDR may be considered as intermediate damage state, and 1% ResISDR is equivalent to collapse damage. In terms of damage state (DS) associated with MaxISDR, FEMA (2000) considered 1%, 2%, and 3% of MaxISDR as Immediate Occupancy, Life Safety, and Collapse Prevention, respectively, for wood shear walls. NBCC (2005) requires the maximum drift of 2.5% to achieve life-safety performance. Goda (2015) used four DSs of wood-frame houses using the UBC-SAWS model associated with MaxISDR of 0.5%, 1%, 2%, and 3%, while the collapse state was defined as MaxISDR>8%. Christovasilis *et al.* (2009) defined the collapse state of the SAWS model with MaxISDR>7%.

In this study, five damage states $DS_{0\sim4}$ are adopted in terms of ResISDR and MaxISDR (Table 1). ResISDR and MaxISDR larger than 7% are considered to be in collapse state.

Table 1. Summary of the damage state from 0 to 4 with ResISDR and MaxISDR.

	DS_0	DS_1	DS_2	DS_3	DS_4
ResISDR	0.01%	0.3%	1%	4%	7%
MaxISDR	0.01%	1%	2%	4%	7%

Since the real mainshock-aftershock records are used in this study, the IM of the mainshock records is higher than that of the aftershock records. For this reason, the mainshock fragility curve and aftershock fragility curves are fitted separately. The function of mainshock fragility

curve fitting is the same as the study by Baker (2015) using the lognormal cumulative distribution $P\ (IM) = \Phi(\ln(IM/\theta)/\beta)$.

Based on the plot of pre-ResISDR, Sa(T=0.3s) and post-MaxISDR of aftershock records in Figure 5, the following procedure is implemented to develop the aftershock fragility curves:

- For each pre-DS_i (i = 0, 1, 2, and 3), the number of post-MaxISDR>post-DS_i (i = 1, 2, 3, and 4) (i.e., exceeding the damage threshold of 0.01%, 1%, 2%, 4%, and 7%, respectively) is counted.
- To fit a fragility curve in a robust manner, the IM bin is defined such that the same number of data points is available. The number of data points in each bin is 5% of the total points given the same pre-DS but is constrained in the range of 50 - 200.
- The same lognormal cumulative distribution function is used by following Baker (2015).

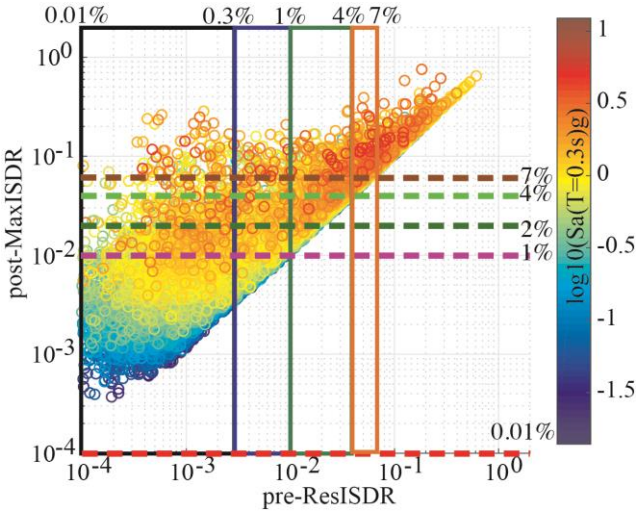

Figure 5. Plot of post-MaxISDR against pre-ResISDR with DS_0(0.01%), DS_1(0.3%), DS_2(1%), DS_3(4%), DS_4(7%). The Sa(T=0.3) is color-coded.

The median (θ) and the standard deviation (β) of the mainshock-aftershock fragility curves of Houses 1-4 are summarized in Table 2.

Table 2.Median values (θ) of mainshock-aftershock fragility curves (standard deviations (β) are shown in the parentheses).

House 1	post-DS_1	post-DS_2	post-DS_3	post-DS_4
pre-DS_0 (MS)	1.5918 (0.3694)	2.6392 (0.4789)	4.1314 (0.6099)	4.9812 (0.7086)
pre-DS_0(AS)	1.8598 (0.5475)	3.599 0(0.5910)	5.3489 (0.5435)	6.1213 (0.5363)
pre-DS_1		1.7311 (1.1020)	4.6237 (1.1339)	10.2059 (1.0561)
pre-DS_2			1.3065 (1.3920)	5.2942 (0.9148)
pre-DS_3				1.8844 (1.2918)
House 2				
pre-DS_0 (MS)	1.3219 (0.4579)	2.0761 (0.5726)	3.1458 (0.7429)	3.7396 (0.8270)
pre-DS_0(AS)	1.7032 (0.6119)	3.3224 (0.6773)	5.9535 (0.7751)	7.2072 (0.7964)
pre-DS_1		1.6149 (1.8484)	8.1321 (2.0116)	9.9679 (1.2132)
pre-DS_2			1.3633 (1.4007)	6.3678 (1.1035)
pre-DS_3				1.6245 (1.3752)
House 3				
pre-DS_0 (MS)	1.2324 (0.4850)	2.0448 (0.5844)	2.9645 (0.7333)	3.5560 (0.8369)
pre-DS_0(AS)	1.6213 (0.6168)	3.2991 (0.7042)	5.8240 (0.7927)	6.8908 (0.7909)
pre-DS_1		1.7070 (1.3421)	7.1208 (1.4396)	8.4547 (1.1416)
pre-DS_2			1.4691 (1.5385)	8.3924 (1.3947)
pre-DS_3				1.7145 (1.1953)
House 4				
pre-DS_0 (MS)	0.9739 (0.5569)	1.5850 (0.6387)	2.1328 (0.7563)	2.6713 (0.8786)
pre-DS_0(AS)	1.4594 (0.6727)	3.1599 (0.7927)	5.2503 (0.8130)	6.7314 (0.7848)
pre-DS_1		1.3766 (1.2135)	4.9196 (1.3994)	14.313 (1.6169)
pre-DS_2			1.5382 (1.5104)	10.0997 (1.5727)
pre-DS_3				1.6060 (1.2268)

3.4. Risk assessment

In total, 6710 houses are considered for the seismic risk assessment for the City of Victoria. By integrating the daily hazard rates and the fragility curves from Sections 3.2 and 3.3, respectively, the probability distributions of damage states for different durations are

evaluated for each house type. Figure 6 shows the normalized number of Houses 1-4 for mainshock only, and durations of 1-week, 1-month, and 1-year after the mainshock. Since House 4 takes up almost 90% of the wood-frame houses, this type is susceptible to major damage. Additional 1.7%, 2.2%, and 3.3% of House 4 are collapsed (DS_4) 1-week, 1-month, and 1-year after the mainshock, in comparison with the normalized number of collapsed houses by the mainshock (5.8%). Considering the total number of Houses 4 is 5869, this suggests additional 99 Houses 4 could collapse in the first week after the mainshock.

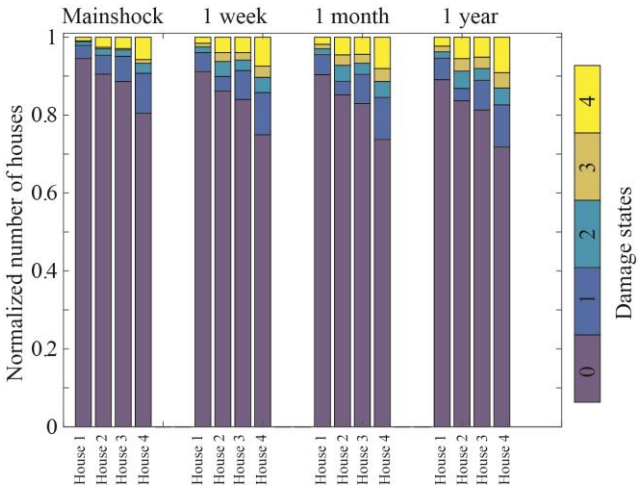

Figure 6. The average number of damaged Houses 1-4 at time intervals mainshock only, 1-week, 1-month, and 1-year.

4. CONCLUSIONS

This study conducted a spatiotemporal seismic hazard and risk analysis for the City of Victoria due to a M9 mainshock. The synthetic catalogs were generated by the ETAS model and further applied to GMPEs to calculate the daily hazard rate at different sites. To estimate the effect of aftershocks on the cumulative damage, the aftershock fragility curves were developed. According to the results, additional 99 House 4 (non-seismically designed) could collapse after 1 week.

In the future study, other observed M9 sequences should be assessed to evaluate the sensitivity of the earthquake risk assessment to the ETAS parameters and other applicable GMPEs. In addition, different IMs and EDPs can be considered in future for the aftershock fragility modeling, and more building types can be included in the risk assessment.

5. ACKNOWLEDGEMENT

This work is supported by the Leverhulme Trust (RPG-2017-006) and the Canada Research Chair in Multi-Hazard Risk Assessment program at Western University (950-232015).

6. REFERENCES

Abrahamson, N., Gregor, N., and Addo, K. (2016). "BC Hydro ground motion prediction equations for subduction earthquakes." *Earthquake Spectra*, 32(1), 23–44.

Allen, T. I., and Wald, D. J. (2009). "On the use of high-resolution topographic data as a proxy for seismic site conditions (VS 30)." *Bulletin of the Seismological Society of America*, 99(2A), 935–943.

Baker, J. W. (2015). "Efficient analytical fragility function fitting using dynamic structural analysis." *Earthquake Spectra*, 31(1), 579–599.

Boore, D. M., Stewart, J. P., Seyhan, E., and Atkinson, G. M. (2014). "NGA-West2 equations for predicting PGA, PGV, and 5% damped PSA for shallow crustal earthquakes." *Earthquake Spectra*, 30(3), 1057–1085.

Christovasilis, I. P., Filiatrault, A., Constantinou, M. C., and Wanitkorkul, A. (2009). "Incremental dynamic analysis of woodframe buildings." *Earthquake Engineering & Structural Dynamics*, 38(4), 477–496.

Ebrahimian, H., Jalayer, F., Asprone, D., Lombardi, A. M., Marzocchi, W., Prota, A., and Manfredi, G. (2014). "A performance-based framework for adaptive seismic aftershock risk assessment." *Earthquake Engineering & Structural Dynamics*, 43(14), 2179–2197.

Federal Emergency Management Agency (FEMA). (2000). "Prestandard and commentary for the seismic rehabilitation of buildings." FEMA.

Folz, B., and Filiatrault, A. (2004). "Seismic analysis of woodframe structures. I: Model formulation." *Journal of Structural Engineering*, 130(9), 1353–1360.

Goda, K. (2015). "Record selection for aftershock incremental dynamic analysis." *Earthquake Engineering & Structural Dynamics*, 44(7),

1157–1162.

Goda, K., and Atkinson, G. M. (2010). "Intraevent spatial correlation of ground-motion parameters using SK-net data." *Bulletin of the Seismological Society of America*, 100(6), 3055–3067.

Goda, K., Atkinson, G. M., and Hong, H. P. (2011). "Seismic loss estimation of wood-frame houses in south-western British Columbia." *Structural Safety*, 33(2), 123–135.

Goda, K., and Salami, M. R. (2014). "Inelastic seismic demand estimation of wood-frame houses subjected to mainshock-aftershock sequences." *Bulletin of Earthquake Engineering*, 12(2), 855–874.

Goda, K., and Taylor, C. A. (2012). "Effects of aftershocks on peak ductility demand due to strong ground motion records from shallow crustal earthquakes." *Earthquake Engineering & Structural Dynamics*, 41(15), 2311–2330.

Goda, K., Wenzel, F., and De Risi, R. (2015). "Empirical assessment of non-linear seismic demand of mainshock-aftershock ground-motion sequences for Japanese earthquakes." *Frontiers in Built Environment*, 1, 6.

Goldfinger, C., Nelson, C. H., Morey, a. E., Joel E, J., Patton, J., Karabanov, E., Gutierrez-Pastor, J., Eriksson, A., Gracia, E., Dunhill, G., Enkin, R., Dallimore, A., and Valiier, T. (2012). "Turbidite Event History — Methods and Implications for Holocene Paleoseismicity of the Cascadia Subduction Zone." *U.S. Geological Survey Professional Paper 1661-F*, (1), 170 p.

Iervolino, I., Giorgio, M., and Chioccarelli, E. (2014). "Closed-form aftershock reliability of damage-cumulating elastic-perfectly-plastic systems." *Earthquake Engineering & Structural Dynamics*, 43(4), 613–625.

Li, Q., and Ellingwood, B. R. (2007). "Performance evaluation and damage assessment of steel frame buildings under main shock--aftershock earthquake sequences." *Earthquake Engineering & Structural Dynamics*, 36(3), 405–427.

Luco, N., Bazzurro, P., and Cornell, C. A. (2004). "Dynamic versus static computation of the residual capacity of a mainshock-damaged building to withstand an aftershock." *13th World Conference on Earthquake Engineering*, (2405).

Nazari, N., Van De Lindt, J. W., and Li, Y. (2013). "Effect of mainshock-aftershock sequences on woodframe building damage fragilities." *Journal of Performance of Constructed Facilities*, 29(1), 4014036.

NBCC. (2005). *National building code of Canada*. Associate Committee on the National Building Code, National Research Council.

Petersen, M. D., Moschetti, M. P., Powers, P. M., Mueller, C. S., Haller, K. M., Frankel, A. D., Zeng, Y., Rezaeian, S., Harmsen, S. C., Boyd, O. S., Field, N., Chen, R., Rukstales, K. S., Luco, N., Wheeler, R. L., Williams, R. A., and Olsen, A. H. (2014). "Documentation for the 2014 Update of the United States National Seismic Hazard Maps." *U.S. Geological Survey Open-File Report*, 243 p.

Raghunandan, M., Liel, A. B., and Luco, N. (2015). "Aftershock collapse vulnerability assessment of reinforced concrete frame structures." *Earthquake Engineering & Structural Dynamics*, 44(3), 419–439.

Seif, S., Mignan, A., Zechar, J. D., Werner, M. J., and Wiemer, S. (2017). "Estimating ETAS: the effects of truncation, missing data, and model assumptions." *Journal of Geophysical Research: Solid Earth*, 122(1), 449–469.

Uma, S. R., Pampanin, S., and Christopoulos, C. (2010). "Development of probabilistic framework for performance-based seismic assessment of structures considering residual deformations." *Journal of Earthquake Engineering*, 14(7), 1092–1111.

Ventura, C. E., Liam Finn, W. D., Onur, T., Blanquera, A., and Rezai, M. (2005). "Regional seismic risk in British Columbia : classification of buildings and development of damage probability functions." *Canadian Journal of Civil Engineering*, 32(2), 372–387.

White, T. W., and Ventura, C. E. (2006). "Seismic performance of wood-frame residential construction in British Columbia." *Earthquake Engineering Research Facility Rep. No. 06*, 3.

Zhang, L., Werner, M. J., and Goda, K. (2018). "Spatiotemporal seismic hazard and risk assessment of aftershocks of M 9 megathrust earthquakes." *Bulletin of the Seismological Society of America*, 108(6), 3313–3335.